Forschungszentrum Karlsruhe
Technik und Umwelt

Wissenschaftliche Berichte
FZKA 6275

Neutron Capture Cross Section of ^{232}Th

K. Wisshak, F. Voss, F. Käppeler
Institut für Kernphysik

August 1999

FORSCHUNGSZENTRUM KARLSRUHE

Technik und Umwelt

Wissenschaftliche Berichte

FZKA 6275

NEUTRON CAPTURE CROSS SECTION OF ^{232}Th

K. WISSHAK, F. VOSS, and F. KÄPPELER

Institut für Kernphysik

Forschungszentrum Karlsruhe GmbH, Karlsruhe
1999

Als Manuskript gedruckt

Forschungszentrum Karlsruhe GmbH
Postfach 3640, 76021 Karlsruhe

Mitglied der Hermann von Helmholtz-Gemeinschaft
Deutscher Forschungszentren (HGF)

ISSN 0947-8620

ABSTRACT

The neutron capture cross section of ^{232}Th has been measured in the energy range from 5 to 225 keV at the Karlsruhe 3.75 MV Van de Graaff accelerator relative to the gold standard. Neutrons were produced via the ^{7}Li$(p,n)^{7}$Be reaction by bombarding metallic Li targets with a pulsed proton beam and capture events were registered with the Karlsruhe 4π Barium Fluoride Detector. The main difficulty in this experiment is the detection of true capture events characterized by a comparably low binding energy of 4.78 MeV in the presence of the high-energy γ-background (up to 3.96 MeV) associated with the decay chain of the natural thorium sample. With the high efficiency and the good energy resolution of the 4π detector the sum energy peak of the capture cascades could be reliably separated from the background over the full range of the neutron spectrum, yielding cross section uncertainties of about 2% above 20 keV and of 4% at 5 keV. The clear identification of the various background components represents a significant improvement compared to existing data for which sometimes high accuracy was claimed, but which were found to be severely discrepant. A comparison to the evaluated files shows reasonable agreement in the energy range above 15 keV, but also severe discrepancies of up to 40% at lower neutron energies.

ZUSAMMENFASSUNG

DER NEUTRONENEINFANGQUERSCHNITT VON ^{232}Th.

Der Neutroneneinfangquerschnitt von ^{232}Th wurde im Energiebereich von 5 bis 225 keV am Karlsruher Van de Graaff Beschleuniger relativ zum Gold–Standardquerschnitt gemessen. Neutronen wurden über die ^{7}Li(p,n)^{7}Be–Reaktion durch Beschuß metallischer Li–Targets mit einem gepulsten Protonenstrahl erzeugt, und Einfangereignisse mit dem Karlsruher 4π Barium Fluorid Detektor nachgewiesen. Die Hauptschwierigkeit des Experimentes war der Nachweis echter Einfangereignisse, die durch eine vergleichsweise niedrige Bindungsenergie von 4.78 MeV charakterisiert sind, gegenüber dem hochenergetischen γ–Untergrund (bis 3.96 MeV) aus der Zerfallskette der natürlichen Thoriumprobe. Die hohe Ansprechwahrscheinlichkeit und die gute Energieauflösung des Detektors erlaubten es jedoch, die vollständig nachgewiesenen Einfangereignisse für alle Neutronenenergien sicher vom Untergrund abzutrennen, und so den Wirkungsquerschnitt oberhalb von 20 keV mit einer Genauigkeit von etwa 2% und bei 5 keV noch mit 4% zu bestimmen. Die saubere Identifizierung der verschiedenen Untergrundkomponenten stellt eine wesentliche Verbesserung im Vergleich zu früheren Messungen dar, für die zwar oft eine hohe Genauigkeit angegeben wurde, die aber sehr unterschiedliche Ergebnisse lieferten. Ein Vergleich mit den evaluierten Datensätzen zeigt eine zufriedenstellende Übereinstimmung im Energiebereich oberhalb von 15 keV, aber Abweichungen bis zu 40% bei niedrigeren Neutronenenergien.

Contents

1 INTRODUCTION

In recent years, reactor concepts based on the ^{232}Th and ^{233}U fuel cycle have received renewed interest [1] since they allow nuclear energy generation without producing significant amounts of plutonium and of higher actinides. Operated as accelerator driven systems (ADS), such reactors can be used to incinerate the wastes of the first generation of nuclear power plants [2, 3, 4]. Since such hybrid systems are subcritical they may also receive better public acceptance.

More detailed ADS studies [5] revealed a significant lack of reliable nuclear data. In particular, the status of the important capture cross section of ^{232}Th was recently claimed to be far from the requested accuracy of 2% [6]. Though there are many experimental data sets quoted with uncertainties of 1-5%, the individual data are discrepant to within 40%. Even if some of these experiments were performed with chemically purified [7] or even isotopically enriched samples [8, 9], where the background due to the decay of the daughter nuclei is partly avoided, the problem of the low binding energy of ^{232}Th of only 4.78 MeV persisted. Hence, experiments using the pulse height weighting technique are susceptible to systematic uncertainties. From this point of view new experiments using a completely different technique are necessary to clarify the existing discrepancies.

In this situation a collaborative effort between IRMM Geel and FZK Karlsruhe was started to remeasure the capture cross section of ^{232}Th from the eV range up to about 200 keV neutron energy. The Karlsruhe setup is very well suited for cross section measurements in the unresolved resonance region as has been demonstrated by the determination of more than 40 (n,γ) cross sections related to nuclear astrophysics. The high efficiency of 97% for capture events allows to use comparably small samples of $\sim$1g, thus avoiding sizeable corrections for multiple scattering and resonance self-shielding. The good energy resolution in combination with the 4π geometry provide a clear discrimination between the sum energy signal of capture events concentrated at the binding energy and the experimental backgrounds. This holds in particular in the neutron energy range between 50 and 200 keV where the signal to background ratio is high enough to allow also in the present case for an overall accuracy of $<$2% in spite of the additional background from the radioactivity of the sample. The good energy resolution is also important for background subtraction, which can be reliably tested via the pronounced lines in the background spectrum.

In the resolved resonance region, the energy depedence of the cross section will be measured at IRMM Geel via the conventional pulse height weighting technique. These results can be normalized in the overlapping energy region from 5 to 20 keV, thus establishing an accurate data set over the entire neutron energy range. The measurements with the Karlsruhe setup and the subsequent data analysis are described in Secs. 2 and 3, followed by a discussion of the results and uncertainties in Secs. 4 and 5.

2 EXPERIMENT

A detailed discussion of the experimental method for the neutron capture cross section measurement with the Karlsruhe 4π BaF_2 detector has been given elsewhere [9, 10, 11, 12]. Therefore, only a general description is given here with emphasis on the specific features of the present measurement on ^{232}Th.

Neutrons were produced via the ^{7}Li$(p,n)^7$Be reaction by bombarding metallic Li targets with the pulsed proton beam of the Karlsruhe 3.75 MV Van de Graaff accelerator. The neutron energy was determined by time of flight (TOF), the samples being located at a flight path of 79 cm. The relevant parameters of the accelerator were a pulse width of <1 ns, a repetition rate of 250 kHz, and an average beam current of 2.1 μA. In different runs, the proton energies were adjusted 30 and 100 keV above the threshold of the ^{7}Li$(p,n)^7$Be reaction at 1.881 MeV, resulting in continuous neutron spectra from 5 to 100 keV, and 5 to 225 keV, respectively. The spectrum with 100 keV maximum neutron energy offers a significantly better signal-to-background ratio at lower energies.

Capture events were registered with the Karlsruhe 4π Barium Fluoride Detector via the prompt capture γ–ray cascades. This detector consists of 42 hexagonal and pentagonal crystals forming a spherical shell of BaF_2 with 10 cm inner radius and 15 cm thickness. It is characterized by a resolution in γ–ray energy of 7% at 2.5 MeV, a time resolution of 500 ps, and a peak efficiency of 90% at 1 MeV. The 1.5 MeV threshold in γ–ray energy used in the present experiment corresponds to an efficiency for capture events of more than 97% for the thorium sample in spite of the low binding energy of only 4.8 MeV. A comprehensive description of this detector can be found in Ref. [11].

The experiment was divided into three runs, two using the conventional data acquisition technique with the detector operated as a calorimeter, and one with an ADC system coupled to the detector for analyzing the signals from all modules individually. In this way, the full spectroscopic information recorded by the detector can be recovered.

The thorium samples were metallic disks with 15 mm diameter. Their gravimetric

Table 1: SAMPLE CHARACTERISTICS

Sample	Diameter	Thickness		Weight	Neutron binding
	(mm)	(mm)	(10^{-3}at/barn)[a]	(g)	energy (MeV)
Empty					
^{232}Th[b]	15.0	0.5	1.5062	1.0256	4.786
^{197}Au[c]	15.0	0.4	2.2478	1.2992	6.513
Graphite	15.0	1.5	13.6103	0.4797	
^{232}Th[d]	15.0	0.9	2.6114	1.7781	4.786
^{197}Au[e]	15.0	0.4	2.2485	1.2996	6.513

[a]Metal samples of natural isotopic composition
[b]Used in Run I
[c]Used in Run I and II
[d]Used in Run II and III
[e]Used in Run III

density of 11.62±0.11 gcm^{-3} being in good agreement with the density of pure metal (11.7 gcm^{-3}) excluded the possibility of partial oxidation and, hence, the corresponding uncertainties in sample definition. Two ^{232}Th samples with different thickness were used in the present experiment in order to check the corrections for neutron multiple scattering and self–shielding.

In addition to the thorium disks, a gold sample was used for measuring the neutron flux. An empty position in the sample ladder served for determination of the sample independent background, and a graphite sample for simulating the background due to scattered neutrons. The sample parameters are listed in Table 1. The neutron transmission of the samples calculated with the SESH code [13] was generally larger than 96% (Table 2), resulting in fairly small sample-related corrections (Sec.3).

During the experiment, the samples were moved cyclically into the measuring position by means of a computer-controlled sample changer. The data acquisition time per sample of about 10 min was defined by integrating the proton beam current to a preselected value. The setup was complemented by two ^{6}Li–glass neutron monitors, one located close to the neutron production target for normalizing the measured spectra of all samples to equal neutron exposure, and the other behind the 4π detector at a flight path of 260 cm for measuring the neutron transmission.

For each event, a 64 bit word was recorded on DAT tape containing the sum energy and TOF information together with 42 bits identifying those detector modules that contributed. The relevant parameters of the three runs are listed in Table 3. The data of Run I were recorded with the ADC system.

Table 2: CALCULATED NEUTRON TRANSMISSION[a]

Sample	Neutron energy (keV)				
	10	20	40	80	160
^{197}Au	0.959	0.965	0.970	0.974	0.979
^{232}Th[b]	0.977	0.979	0.980	0.982	0.983
^{232}Th[c]	0.961	0.964	0.966	0.968	0.971

[a] Monte Carlo calculation with SESH code [13].
[b] Thin sample.
[c] Thick sample.

Table 3: PARAMETERS OF THE INDIVIDUAL RUNS

Run	Flight path (mm)	TOF scale (ns/ch)	Number of cycles	Maximum neutron energy (keV)	Measuring time (d)	Mode of operation	Average beam current (μA)	Threshold in sum energy (MeV)
I	788.0	0.7091	595	100	13.0	ADC	2.4	1.4
II	788.2	0.7600	366	200	8.9	Calorimeter	2.1	1.4
III	787.7	0.7602	592	100	19.5	Calorimeter	1.7	1.5

3 DATA ANALYSIS

The analysis of the accumulated data was carried out in the same way as described previously [9, 10, 12]. All events were sorted into two–dimensional spectra containing 128 sum energy versus 2048 TOF channels according to various event multiplicities (Evaluation 1). In Evaluation 2, this procedure was repeated by rejecting those events, where only neighboring detector modules contributed to the sum energy signal. With this option, background from the natural radioactivity of the BaF_2 crystals and from scattered neutrons can be reduced. For all samples, the resulting spectra were normalized to equal neutron exposure using the count rate of the ^{6}Li glass monitor close to the neutron target. The corresponding normalization factors are below 0.5% for all runs. The treatment of the two–dimensional spectra derived from the data recorded with the ADC system is slightly more complicated and was performed as described in Ref. [9].

In the next step of data analysis, sample–independent backgrounds were removed by subtracting the spectra measured with the empty position in the sample changer. A remaining constant background was determined at very long flight times, where no time–correlated events are expected. In contrast to previous measurements on stable isotopes, most of the time–independent background is caused by the activity of the ^{232}Th sample. This is illustrated in Fig. 1, where this background is shown for different multiplicities (approximated by the number of detector modules contributing to each event). The total background is shown in the first spectrum (m=0). The dashed area represents the background measured in a previous experiment with a stable sample. The background from the thorium sample is dominated by the γ–ray cascades following the β^- decay of ^{208}Tl, which are clearly identified by the sharp lines at 2.6, 3.2, and 3.7 MeV γ-ray energy.

The lines at 3.2 and 3.7 MeV are due to γ–ray cascades with multiplicities two and three, respectively. This explains why their relative intensities differ considerably in the spectra for different multiplicity. Given the non-negligible probability for cross-talking between BaF_2 modules, i.e. that one γ-ray may cause signals in two neighboring crystals, these background lines appear in the spectra with multiplicity four and five as well. Since the 2.6 MeV level in ^{208}Pb is not directly populated by β^- decays of ^{208}Tl, the line at 2.6 MeV appears only if the first transition in this two-step cascade escapes detection. The feature at 1.7 MeV is an artefact caused by the steeply rising background at low energies and the sharp cut-off by the 1.5 MeV threshold. In principle, the background extends up to 3.9 MeV due to a level in ^{208}Pb which is populated with 3% probability, but the corresponding line is too weak to be resolved in the spectra.

The occurence of sharp lines in the background spectrum confirms that the β^- decay electrons, which are emitted in coincidence with the γ–ray cascades, are completely absorbed either in the sample or in the BaF_2 canning and do not affect the detector response. The most important feature in the spectra of Fig. 1 is the absence of significant background at 4.8 MeV, where the sum energy peak of the ^{232}Th capture cascades is expected.

After this first background subtraction, the resulting two–dimensional spectra contain

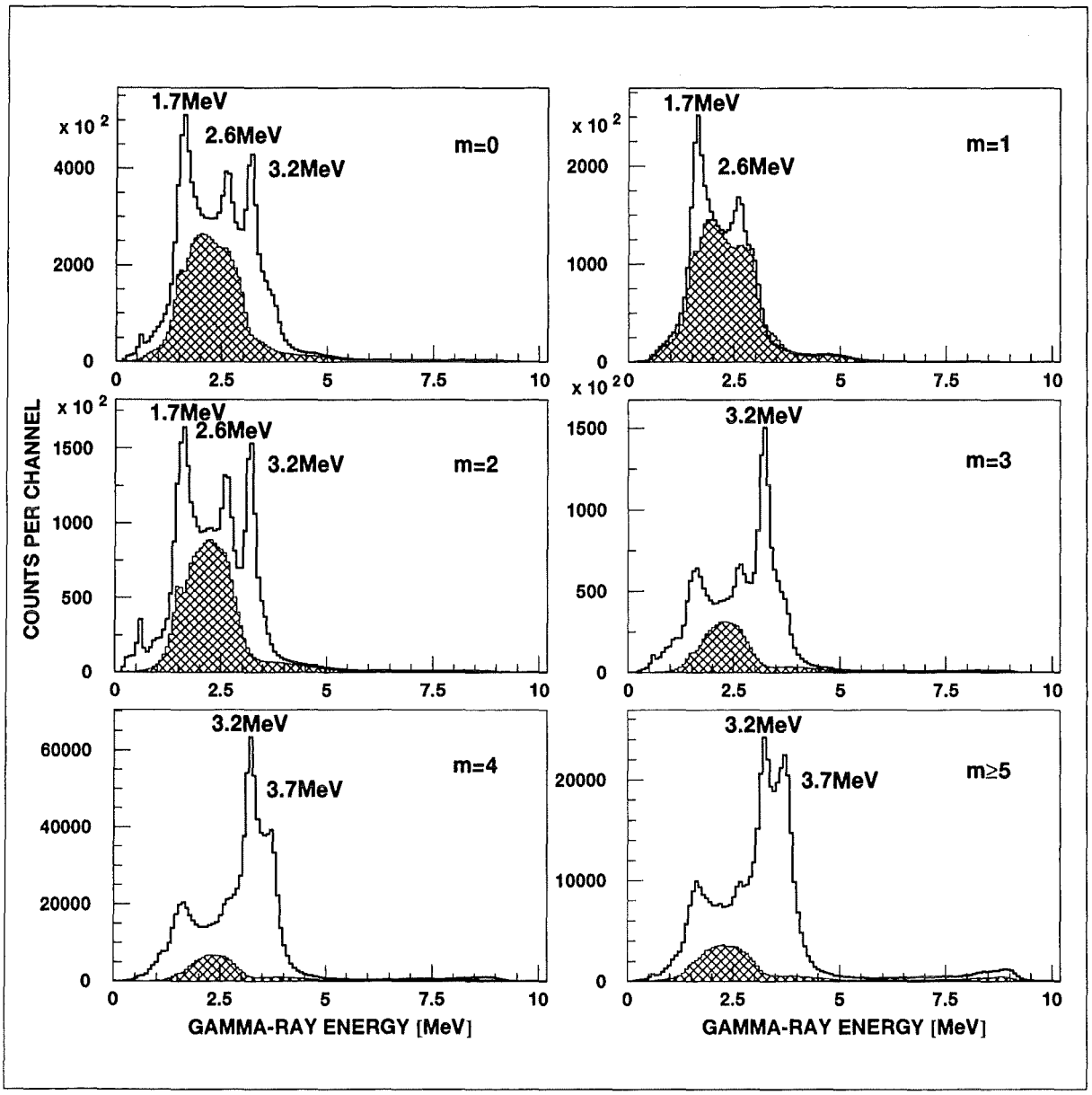

Figure 1: The time-independent background caused by the radioactivity of the thorium sample for different multiplicities. The dashed areas represent the respective background measured with a stable sample.

only events correlated with the interaction of neutrons in the sample (middle part of Fig. 2).

The last step of background subtraction concerns events due to capture of sample scattered neutrons. This effect can be corrected by means of the data measured with the graphite sample. Most of this background is concentrated at higher sum energies and does, therefore, not disturb the ^{232}Th captures (see middle part of Fig. 2). The two broad structures at sum energies of 6.9 and 9.1 MeV, which correspond to capture in the even and odd barium isotopes of the scintillator, are clearly separated from true capture events

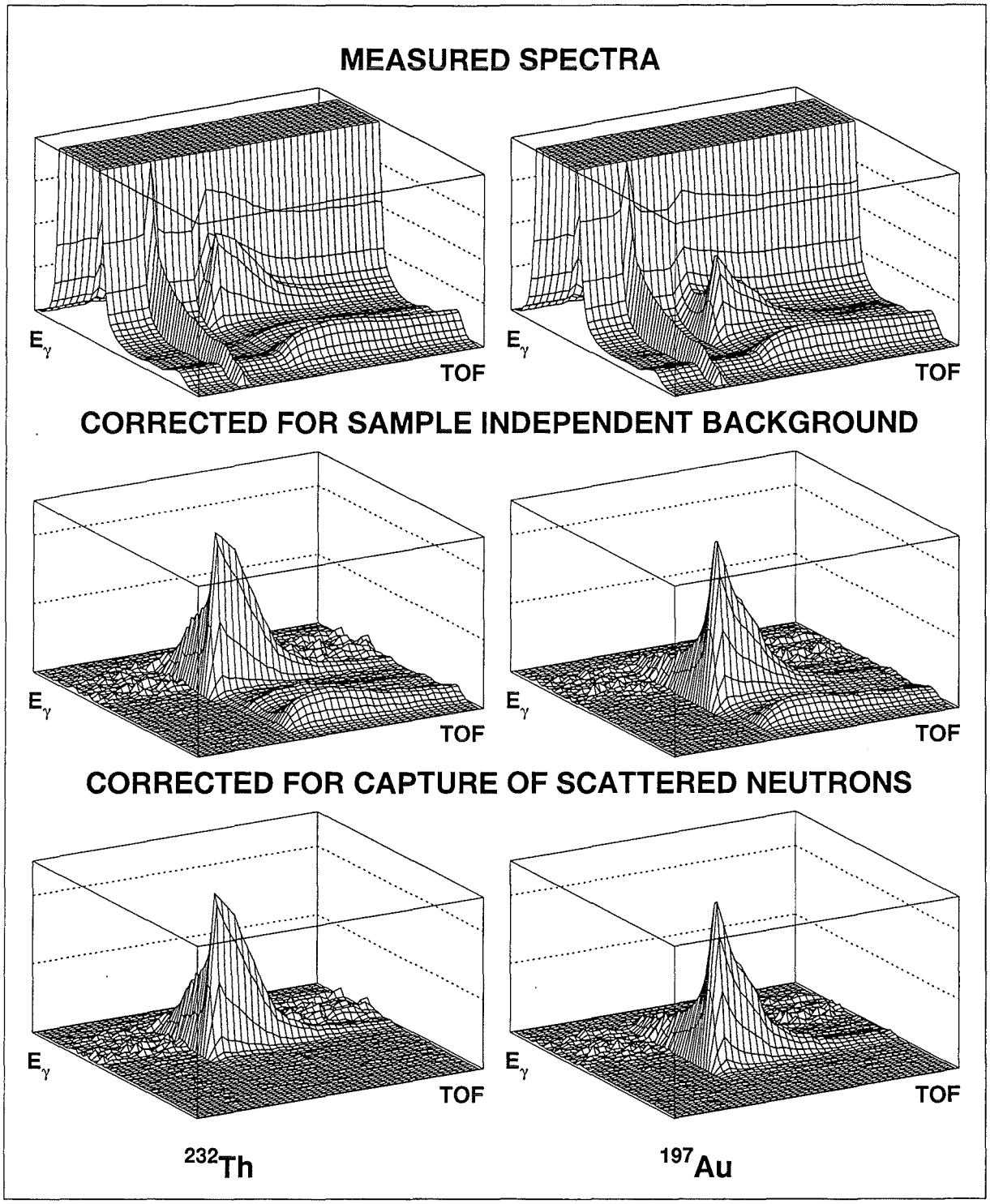

Figure 2: The different steps of background subtraction in the two-dimensional sum energy $\times$ TOF spectra. The data are shown for ^{232}Th and ^{197}Au measured in Run III with 100 keV maximum neutron energy and for multiplicities >2. (The original resolution of 128 $\times$ 2048 channels was compressed into 64 $\times$ 64 channels for better readability).

in ^{232}Th. Based on these structures, the spectum measured with the graphite sample can be normalized in a broad sum energy range from 5.1 to 9.3 MeV. The normalization factor was calculated for each time of flight channel, and shows a significant time-dependence. Due to the favorable ratio of capture to scattering cross section and the low binding energy of thorium this correction is very small. This background is actually indicated in Fig. 3, where the projections of the two-dimensional spectra on the TOF axis are shown before this correction was applied. The corresponding signal/background ratios are listed in Table 4 for different neutron energies and for the two different neutron spectra with 100 and 200 keV maximum energy. Note, that the signal to background ratio is better in the runs with low maximum neutron energy. The final net spectra are shown in the lower part of Fig. 2.

Table 4: SIGNAL/BACKGROUND RATIO FOR RUNS WITH DIFFERENT MAXIMUM NEUTRON ENERGY

Sample	σ_t/σ_γ	Maximum neutron energy	Signal/Background ratio[a]		
	E_n=30 keV	(keV)	E_n=30 keV	E_n=20 keV	E_n=10 keV
^{232}Th	29	100	15.9	6.8	3.6
^{197}Au	24		8.9	4.4	2.9
^{232}Th		200	11.1	6.3	3.3
^{197}Au			6.7	3.7	2.5

[a]Defined as (effect+neutron scattering background)/(neutron scattering background)

After subtraction of the scattering background the cross section shape versus neutron energy was determined from the TOF spectra of Fig. 3. For normalization, the two-dimensional data were projected onto the sum energy axis using the TOF region with optimum signal/background ratio as indicated in Fig. 3 by vertical lines. The resulting pulse height spectra are given in Fig. 4 for events with multiplicities >2. The threshold in sum energy is 1.5 MeV. The figure demonstrates, that the background due to the radioactivity of the sample was properly treated in the normalization interval: the strong lines at 2.6, 3.2, and 3.7 MeV are completely eliminated.

The sum energy spectra are shown in Fig. 5 for different multiplicities. These multiplicities correspond to the number of detector modules contributing per event, which are slightly larger than the true multiplicities because of cross talking. Only 26% of the capture events in thorium are observed with multiplicities $\geq$5, while the respective fraction in gold is 38%. The arrows in Fig. 5 indicate the range of sum energy channels that was integrated to obtain the TOF spectra of Fig. 3 for determining the cross section shape. In contrast to previous mesurements on stable samples, where a broad sum-energy range was accepted for high multiplicities, this range was restricted in the present case to channels above 52. The corresponding energy of 4.2 MeV is well above the background from the radioactivity of the sample (see Fig. 1).

The sum energy spectra of the thorium and gold samples are shown in Figs. 6 and 7 for different neutron energy bins. The dashed areas in the spectra at lower neutron

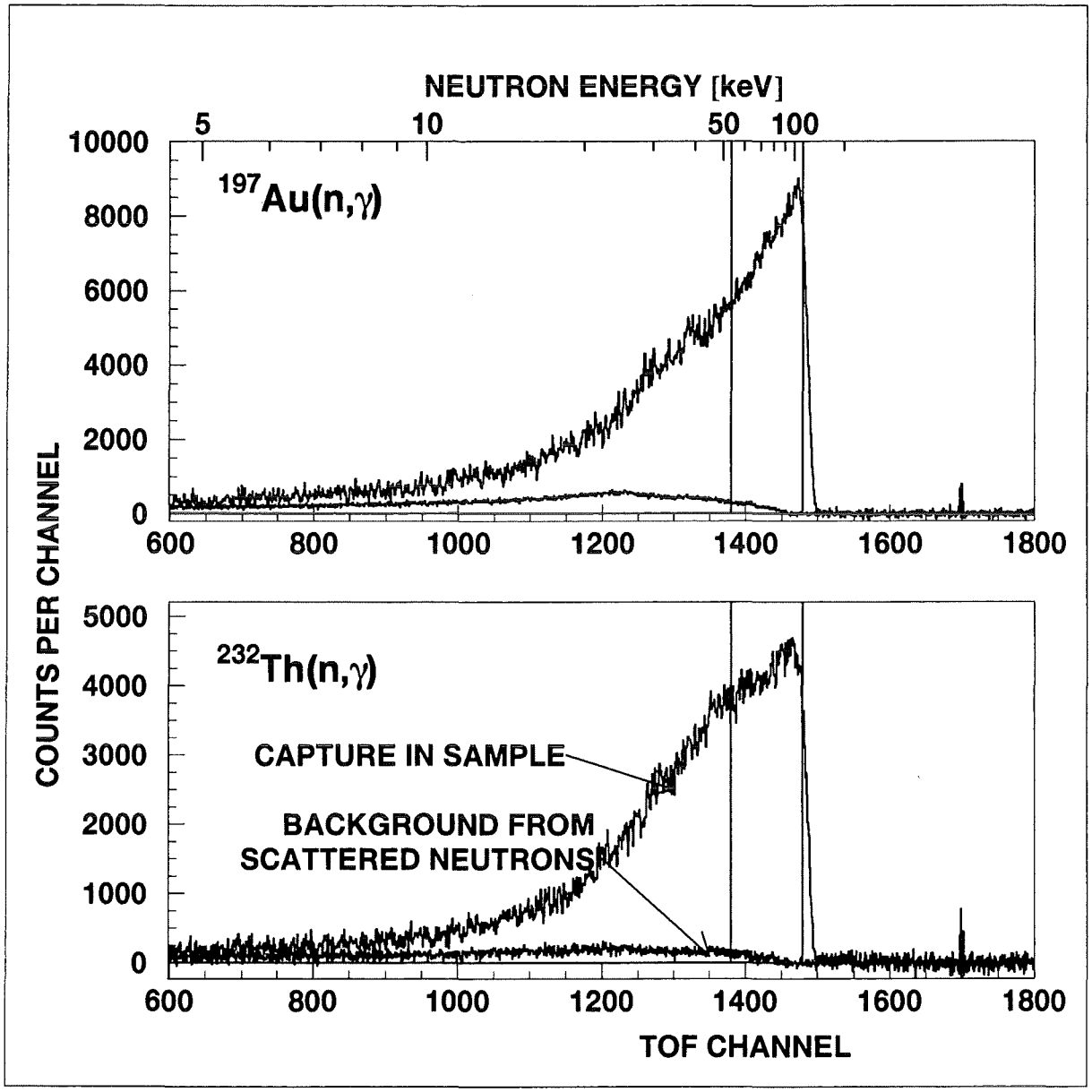

Figure 3: TOF spectra measured in Run III (100 keV maximum neutron energy). The background due to sample scattered neutrons is shown separately. The region used for absolute normalization of the cross section is indicated by vertical lines.

energies correspond to the normalized shape of the spectrum in the first energy interval with the best statistics. These figures demonstrate three important features of the present experiment:

- The shape of the sum energy spectra does not change in the investigated neutron energy range as can best be seen in the spectra of the gold sample which are less affected by backgrounds. This assumption is important for the evaluation of the differential cross section, since its shape is determined from the restricted range in sum energy indicated by the vertical lines.

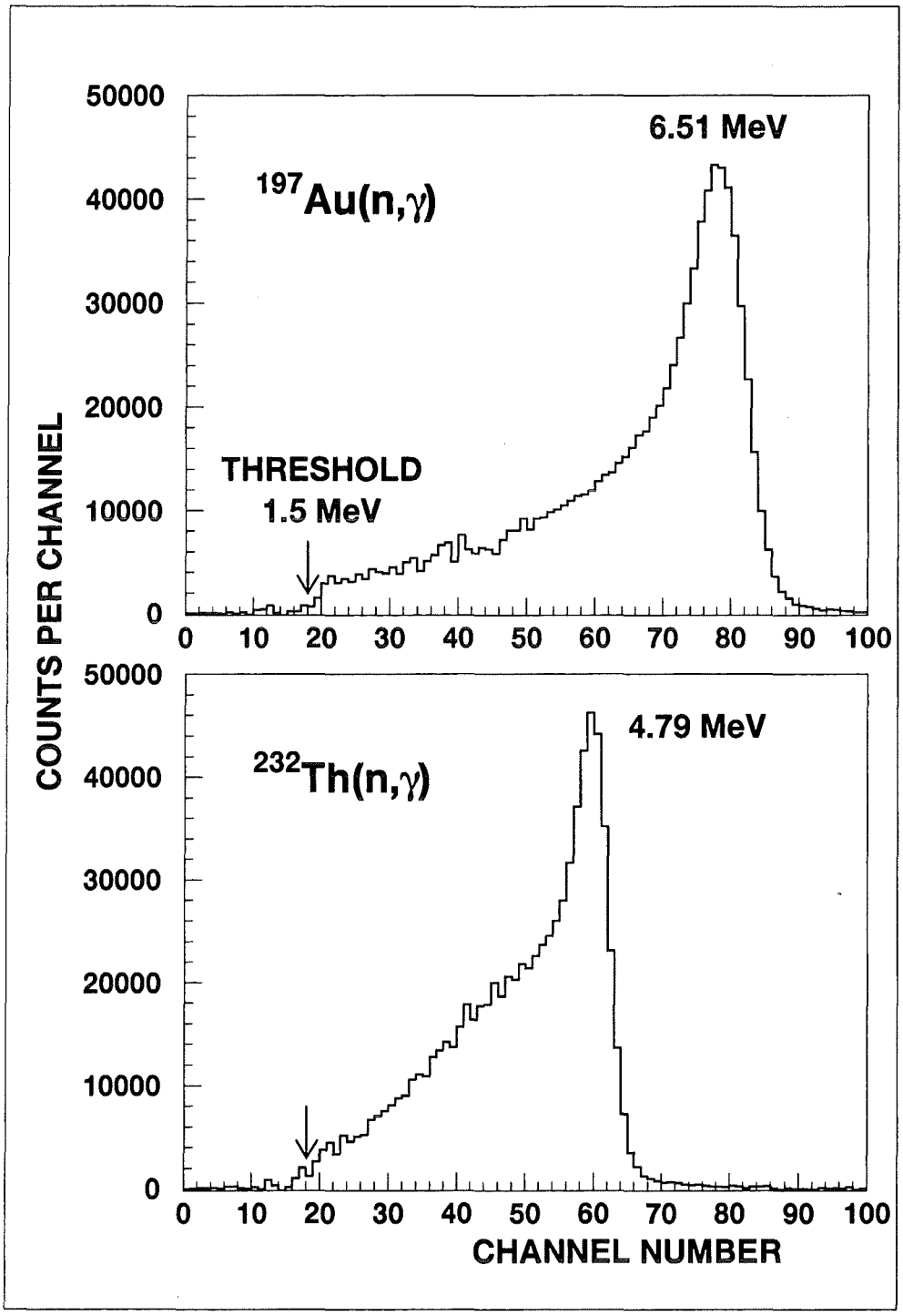

Figure 4: Sum energy spectra measured in Run III containing events with multiplicity >2. These spectra were obtained by projection of the two-dimensional data in the TOF region below the maximum neutron energy as indicated by the vertical lines in Fig. 3.

- The background from the radioactivity of the thorium sample gives rise to large statistical fluctuations. With the above assumption, the final cross section is completely determined from events outside this critical interval and is, therefore, not

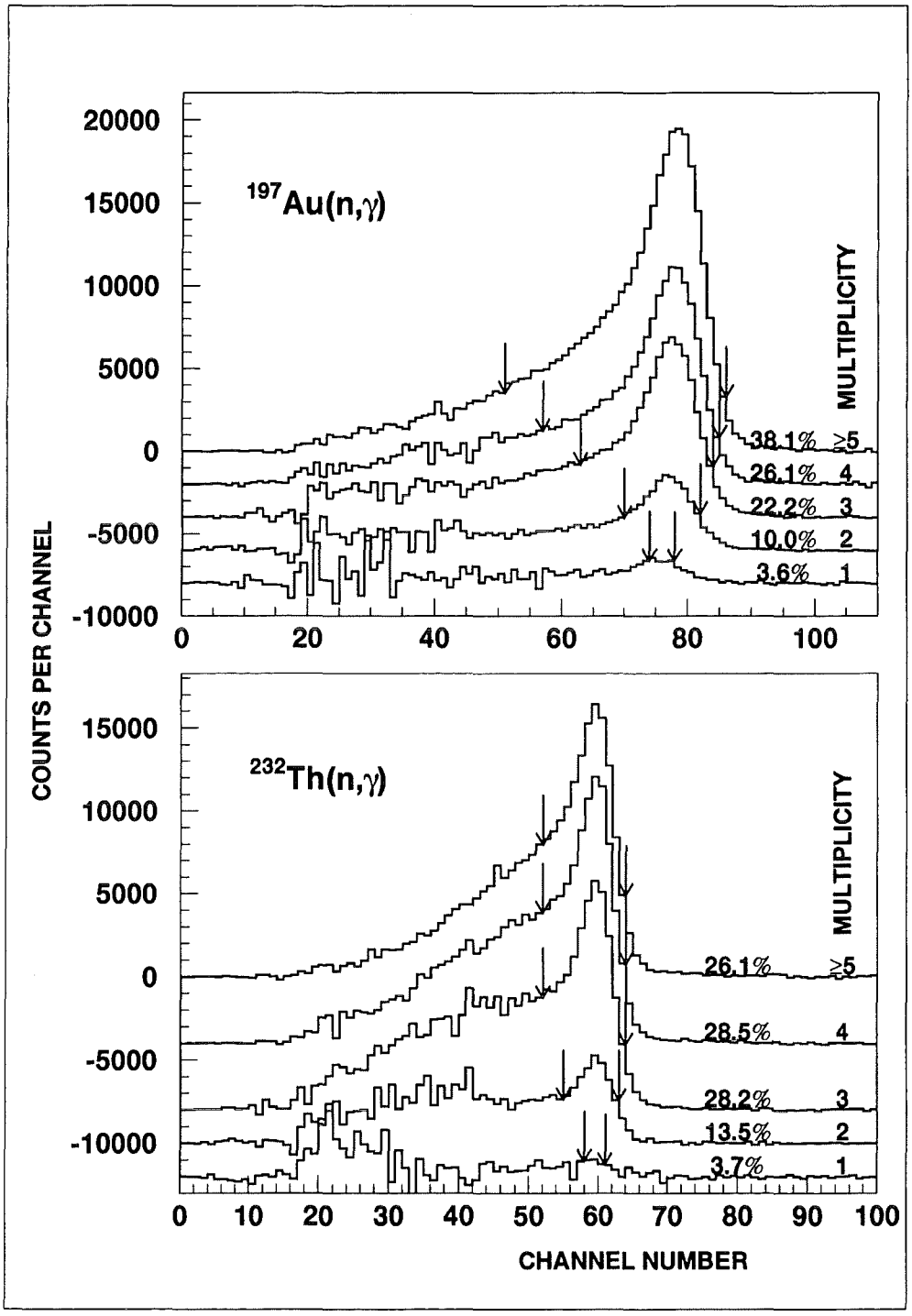

Figure 5: Sum energy spectra as a function of multiplicity. The regions used to determine the cross section shape are indicated by arrows.

affected by these fluctuations. It is to be emphasized that this type of analysis is specific for the 4π BaF_2 detector and can only be applied because of the good resolution in γ–ray energy.

- The energy resolution is even sufficient to allow for the correction of a rather small

effect. The peak position in the sum–energy spectra is determined by the binding energy of the captured neutron complemented by its kinetic energy. Accordingly, a minute peak shift is observed in the lower neutron energy bins compared to the hatched areas, which correspond to the normalized spectrum of the highest bin. Therefore, the relative area in the spectra of capture events is slightly reduced with decreasing neutron energy. This effect was considered in the evaluation, in particular in case of thorium where only a narrow range of the sum–energy spectrum could be used in data analysis.

The cross section ratio of thorium relative to the gold standard is given by

$$\frac{\sigma_i(Th)}{\sigma_i(Au)} = \frac{Z_i(Th)}{Z_i(Au)} \cdot \frac{\Sigma Z(Au)}{\Sigma Z(Th)} \cdot \frac{\Sigma E(Th)}{\Sigma E(Au)} \cdot \frac{m(Au)}{m(Th)} \cdot F_1 \cdot F_2 \cdot F_3. \quad (1)$$

In this expression, Z_i are the count rates in channel i of the TOF spectrum, ΣZ are the TOF rates integrated over the interval used for normalization (as marked in Fig. 3), and ΣE are the total count rates in the sum energy spectra for all multiplicities in this TOF interval. The respective sum energy spectra are shown in Fig. 5. For all multiplicities these spectra were integrated from the threshold at 1.5 MeV beyond the binding energy, and the sum of these results, ΣE is used in Eq. 1. A full description of this procedure is given in Ref.[14]. The quantity m is the sample thickness in atoms/barn. The factor F_1 = (100–f(Au))/(100–f(Th)) corrects for the fraction of capture events f below the experimental threshold in sum energy (see Table 5), F_2 is the ratio of the multiple scattering and self–shielding corrections for gold and thorium, and F_3 accounts for the shift of the full energy peak with neutron energy as mentioned before.

The fraction of unobserved capture events, f, and the correction factors F_1 were calculated as described in Ref. [12]. The input for this calculation are the individual neutron capture cascades and their relative contributions to the total capture cross section as well as the detector efficiency for monoenergetic γ–rays in the energy range up to 10 MeV. This information was derived directly from the experimental data recorded with the ADC system in Run I. From these data, only events close to the sum energy peak (see Fig. 4) were selected, which contain the full capture γ–ray cascade. This ensemble was further reduced by restricting the analysis to the TOF region with optimum signal to background ratio (vertical lines in Fig. 3). The calculated correction factors F_1 are listed in Table 5. The capture γ-ray spectra obtained from the data taken with the ADC system are shown in Fig. 8 in energy bins of 500 keV.

The correction for neutron multiple scattering and self–shielding was obtained with the SESH code [13]. Apart from the pairing energies [15], most of the input parameters were taken from Ref. [16] but were slightly modified in order to reproduce the total and the measured capture cross sections. The final values are listed in Table 6 together with the calculated total cross sections. The resulting correction factors, MS(X) and F_2, are compiled in Table 7. In general, these corrections are below 3%.

The correction F_3 had to be applied since the background from the radioactivity of the thorium sample left only a narrow interval in the sum energy spectrum (indicated in Figs. 5 and 6) that can be used for evaluating the countrate $Z_i(Th)$ in the TOF spectrum. Since the peak in the sum energy spectrum shifts slightly with neutron energy (Fig. 6), the

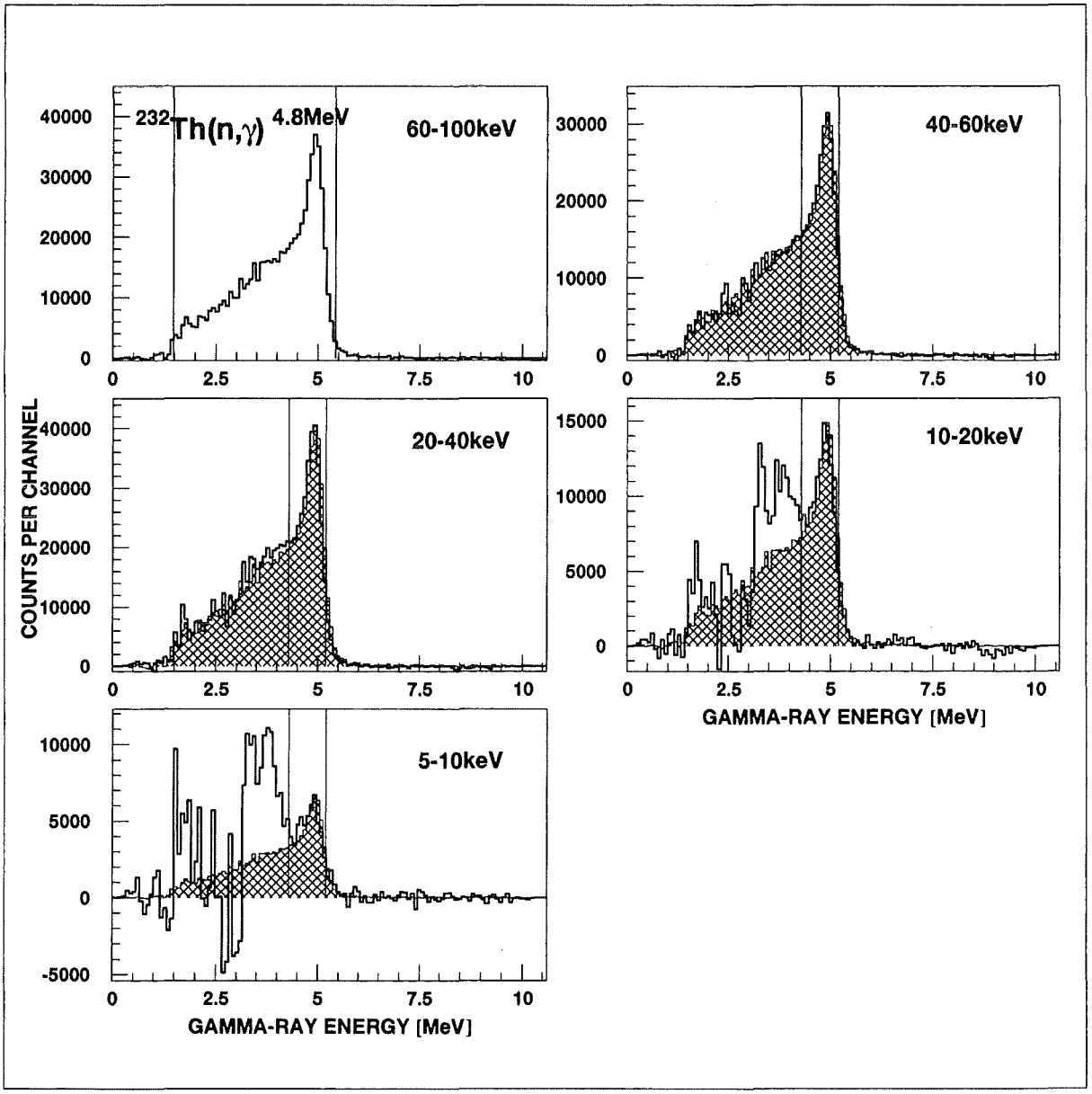

Figure 6: Sum energy spectra as a function of neutron energy. The regions used in the evaluation of the cross section shape are indicated by vertical lines. The hatched areas correspond to the shape of the first spectrum (60-100 keV).

fraction of capture events in this interval changes accordingly. The resulting correction factors f_3 are defined as the ratio of the spectrum fractions in the reference intervals (60 to 100 keV and 100 to 200 keV, respectively) and the various neutron energy intervals. It is determined by fitting the undisturbed sum energy spectra (first spectra in Figs. 6 and 9) with a gaussian for the full energy peak and a truncated polynomial for the tail. By means of this fit, analysis of the other energy intervals provided the corrections listed in Table 8.

In Runs I and III with 100 keV maximum neutron energy this effect is relatively small,

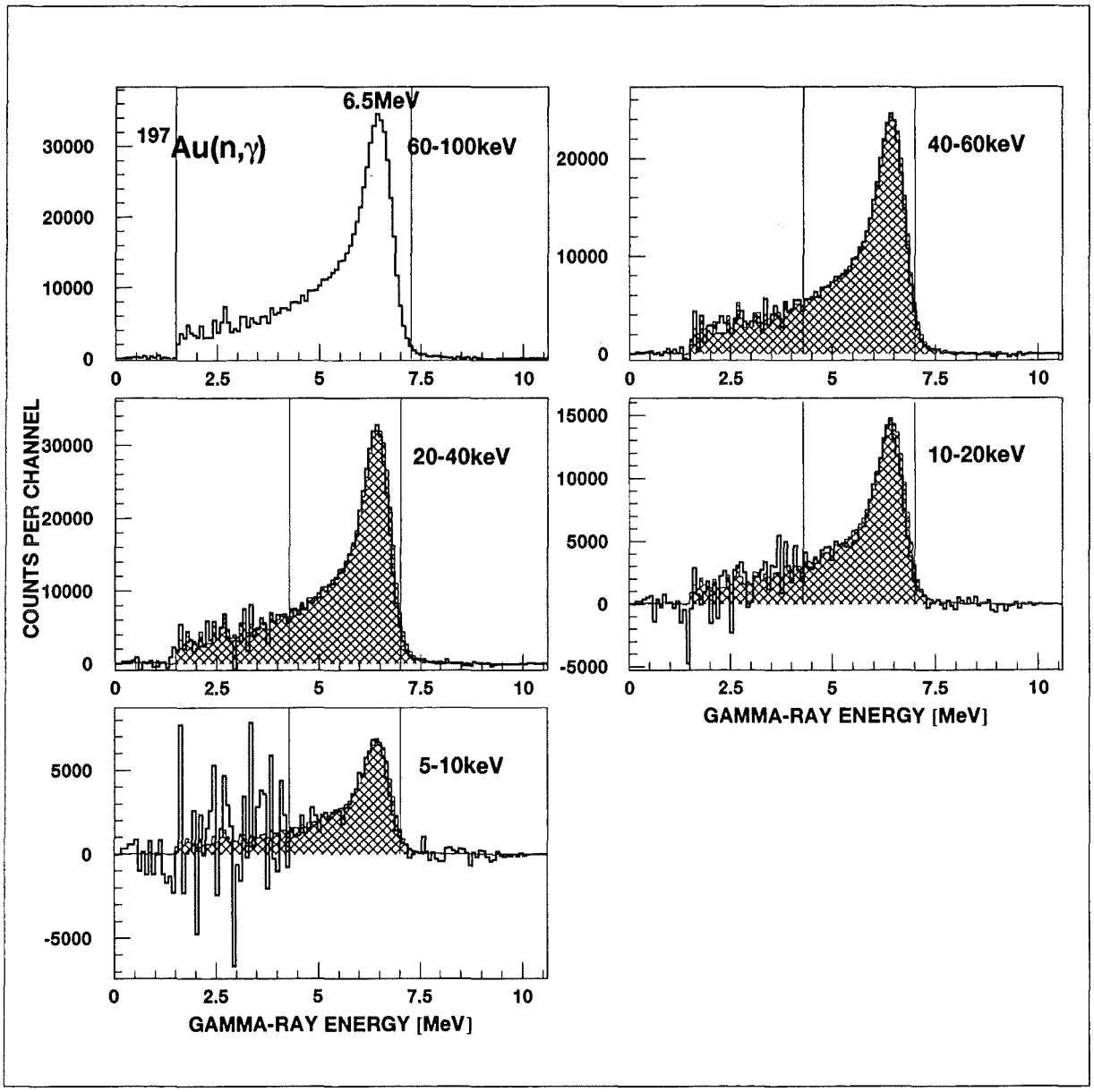

Figure 7: Same as Fig. 6 but for the gold sample.

leading to corrections below 3% even in the lowest energy interval, whereas for Run II with 200 keV maximum neutron energy significantly larger corrections of up to 8% were required. This effect is obvious from Fig. 9, where the shift in the position of the sum energy peak is clearly visible. It has to be noted, however, that also in these spectra, true capture events in the intervals marked by vertical lines are well separated from the background due to the radioactivity of the sample.

The same procedure was repeated for the gold sample. Because a much wider sum energy interval could be used in this evaluation (see Fig. 7), the f_3 corrections are correspondingly smaller and do not exceed 0.2% in Runs I and III and 0.9% in Run II. The final correction factor F_3 is obtained as the ratio of the f_3 values for thorium and gold.

Table 5: FRACTION OF UNDETECTED CAPTURE EVENTS, f (%), AND THE RELATED CORRECTION FACTORS F_1.[a]

	Threshold in Sum Energy (MeV)		
	1.4	1.5	2.0
f(^{197}Au)		4.92	6.85
f(^{232}Th)		3.14	5.47
F_1(^{232}Th/^{197}Au)	0.981	0.982	0.985

[a] derived from capture cascades measured with the ADC system.

The correction for the gold sample is typical for all previous experiments with the Karlsruhe $4\pi BaF_2$ detector. Since only stable samples were used in these cases, the much smaller effect confirms that these corrections were, indeed, negligible, since most of the effect cancels out in the expression for the cross section ratio.

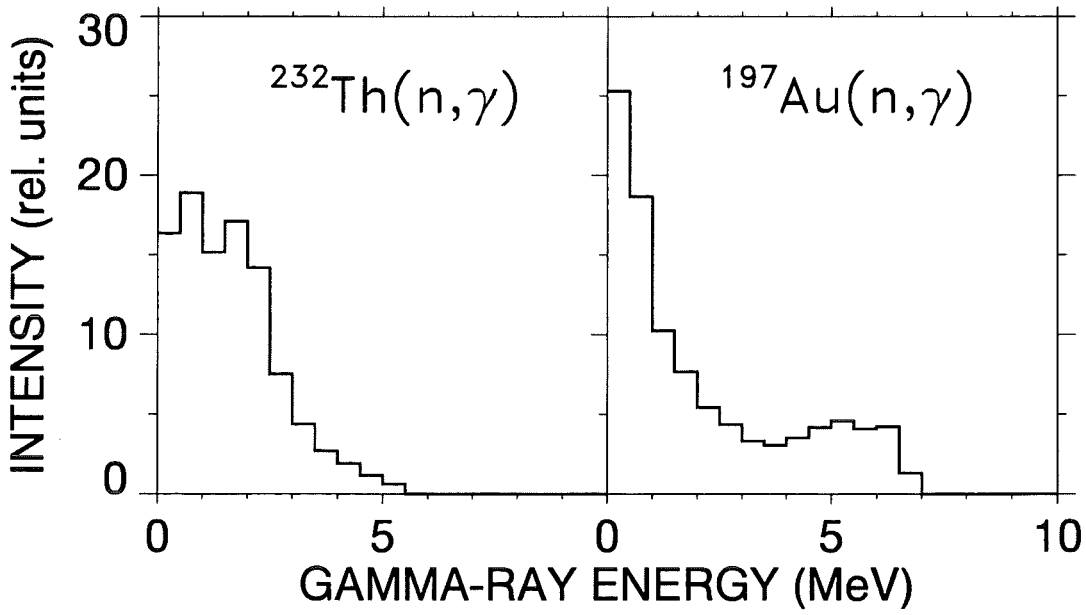

Figure 8: Gamma-ray spectra of capture cascades in thorium and gold obtained from the data taken with the ADC system in Run I.

Table 6: PARAMETERS FOR THE CALCULATION OF NEUTRON SELF-SHIELDING AND MULTIPLE SCATTERING CORRECTIONS

Parameter		^{232}Th	^{197}Au
Nucleon Number		232	197
Binding Energy (MeV)		4.786	6.513
Pairing Energy (MeV)		0.78	0.0
Effective Temperature (K)		293	293
Nuclear Spin		0	1.5
Average Radiation	s	0.040	0.128
Width (eV)	p	0.010	0.048
	d	0.001	0.048
Average Level	s	16.8	16.5
Spacing (eV)	p[a]	5.6	8.25
	d[a]	3.36	5.28
Strength Function	S_0	0.84	2.0
(10^{-4})	S_1	1.48	0.4
	S_2	1.12	0.7
Nuclear Radius	s	9.65	9.5
(fm)	p	9.65	9.5
	d	9.65	9.5
		Calculated total cross sections	
3 keV		18.2	26.1
5 keV		16.7	22.6
10 keV		15.3	18.9
20 keV		14.2	16.1
40 keV		13.3	13.8
80 keV		12.4	11.7
160 keV		11.3	9.64
320 keV		9.82	7.61

[a]Calculated with SESH [13]

Table 7: CORRECTION FACTORS FOR NEUTRON SELF-SHIELDING AND MULTIPLE SCATTERING, MS AND THE CORRECTION FACTOR F_2 FOR THE CROSS SECTION RATIO.

Energy Bin (keV)	MS			F_2 = MS(Au)/MS(X)	
	^{197}Au	^{232}Th thin	^{232}Th thick	^{232}Th/^{197}Au thin	^{232}Th/^{197}Au thick
5 – 7.5	1.016	0.994	0.983	1.022	1.034
7.5 – 10	1.027	0.998	0.989	1.029	1.038
10 – 12.5	1.032	1.000	0.993	1.032	1.039
12.5 –15	1.035	1.002	0.996	1.033	1.039
15 – 20	1.037	1.004	0.999	1.033	1.038
20 – 25	1.037	1.006	1.003	1.031	1.034
25 – 30	1.036	1.008	1.006	1.028	1.030
30 – 40	1.036	1.010	1.009	1.026	1.027
40 – 50	1.035	1.012	1.012	1.023	1.023
50 – 60	1.034	1.014	1.015	1.020	1.019
60 – 80	1.033	1.015	1.017	1.018	1.016
80 – 100	1.032	1.016	1.019	1.016	1.013
100 – 120	1.030	1.017	1.020	1.013	1.010
120 – 150	1.029	1.017	1.021	1.012	1.008
150 – 175	1.029	1.017	1.022	1.012	1.007
175 – 200	1.027	1.017	1.022	1.010	1.005
200 – 225	1.026	1.017	1.022	1.009	1.004
Uncertainty (%)	0.3	0.4	0.4	0.5	0.5

Table 8: CORRECTION FACTORS f_3 FOR THE SHIFT IN THE SUM ENERGY SPECTRUM AND THE CORRECTION FACTOR F_3 FOR THE CROSS SECTION RATIO.

Energy Bin (keV)	f_3(Th)		f_3(Au)		F_3(Th/Au)	
	Run I + III	Run II	Run I + III	Run II	Run I + III	Run II
100 – 200	–	1.0	–	1.0	–	1.0
60 – 100	1.0	1.031	1.0	1.002	1.0	1.029
40 – 60	1.012	1.049	1.001	1.005	1.011	1.044
20 – 40	1.021	1.064	1.001	1.007	1.020	1.057
10 – 20	1.027	1.075	1.002	1.009	1.025	1.065
5 – 10	1.031	1.081	1.002	1.009	1.029	1.071

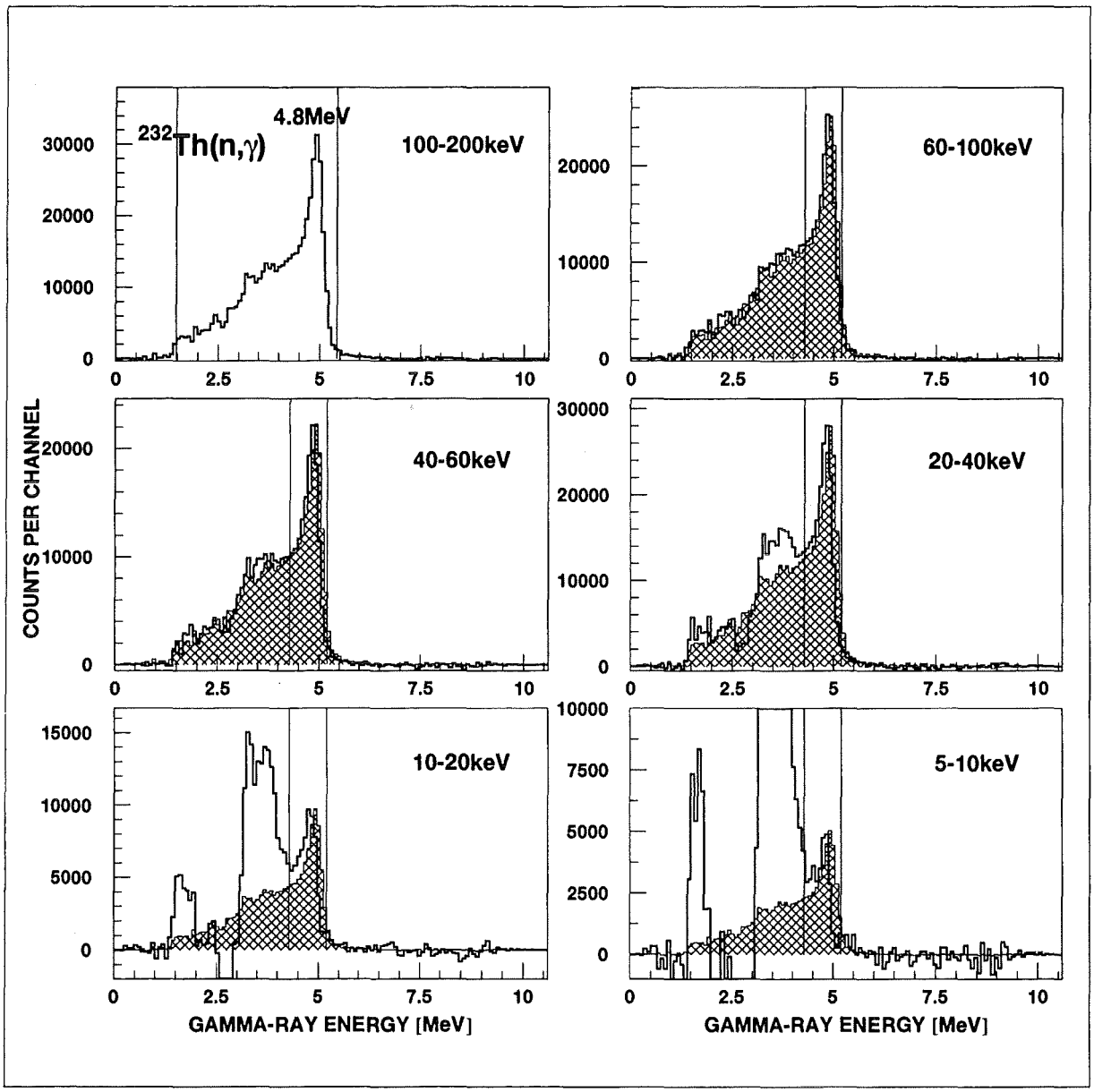

Figure 9: Same as Fig. 6 but for the run with 200 keV maximum neutron energy.

4 THE NEUTRON CAPTURE CROSS SECTION OF ^{232}Th

The final neutron capture cross section ratios of ^{232}Th and ^{197}Au are listed in Table 9 together with the respective statistical uncertainties. The data are given for all runs and for the two evaluation methods discussed in Sec. 3. The last column in each table contains the weighted average, the weight being determined by the inverse of the squared statistical uncertainties. Since the cross section ratios depend weakly on energy, the averages for the energy interval from 30 to 80 keV are also included for better comparison of the individual results. Very good agreement is found for the results of the individual runs. This is an important test since these data sets were obtained with different data acquisition modes, neutron spectra, and sample masses. For the first time, however, a systematic difference of 2.3% remained on average between the results of the two evaluation methods, corresponding to four standard deviations.

As in the previous measurements with the 4π BaF_2 detector [9, 10, 17], the final cross section ratios were adopted from Evaluation 2. The respective mean values are compiled for all runs in Table 10 together with the statistical, systematic, and total uncertainties. The final uncertainties of the cross section ratios are less than 1.7% in the energy range from 20 to 100 keV but reach 4% in the lowest energy bin.

The experimental ratios were converted into absolute cross sections using the gold data of Macklin [18] after normalization by a factor of 0.989 to the absolute value of Ratynski and Käppeler [19] (Table 10). The uncertainties of the resulting values can be obtained by adding the 1.5% uncertainty of the reference cross section to the uncertainties of the respective cross section ratios.

The present results are compared to evaluated files in Figs. 10 to 12. In general, there is good agreement for energies above 15 keV, but at lower energies severe discrepancies were found compared to all evaluated data sets. The present results are best compatible with the JENDL3.2 evaluation, whereas the unphysical step in the JEF2.2 evaluation at 50 keV leads to deviations of about 20% at higher energies. As discussed in Sec. 3, systematic uncertainties due to background subtraction can be excluded in the present case. Also uncertainties of the correction for neutron multiple scattering and self-shielding could be significantly reduced. Therefore, it is rather likely that the severe discrepancies at low neutron energies are due to unidentified or underestimated systematic effects in previous experiments. Instead of a comparison to the individual experimental results we refer to the detailed plots given in Ref. [20], which show that the individual experimental data in the energy range from 5 to 30 keV are nearly homogeniously distributed in a $\pm 30\%$ band around the ENDF-B/V evaluation.

Table 9: $\sigma(^{232}\mathrm{Th})/\sigma(^{197}\mathrm{Au})$ AND STATISTICAL UNCERTAINTIES IN (%)

Energy Bin (keV)	Run I		Run II		Run III		Average	
Evaluation 1								
5 – 7.5	0.6543	9.6	0.9032	9.0	0.7722	6.2	0.7793	4.5
7.5 – 10	0.8474	6.0	0.9086	6.7	0.8654	4.7	0.8701	3.2
10 – 12.5	0.7693	4.7	0.8340	5.2	0.7598	3.8	0.7807	2.6
12.5 – 15	0.8461	3.7	0.9364	4.1	0.8389	3.0	0.8650	2.0
15 – 20	0.8248	2.3	0.8330	2.6	0.8361	1.9	0.8320	1.3
20 – 25	0.9694	1.8	1.0230	1.9	1.0079	1.5	1.0005	1.0
25 – 30	0.9215	1.5	0.9772	1.6	0.9362	1.3	0.9436	0.8
30 – 40	0.9327	1.3	0.9742	1.2	0.9624	1.0	0.9582	0.7
40 – 50	0.9896	1.3	1.0267	1.2	1.0169	1.0	1.0127	0.7
50 – 60	0.9202	1.3	0.9475	1.2	0.9323	1.0	0.9337	0.7
60 – 80	0.8005	1.2	0.8356	1.0	0.8253	0.9	0.8222	0.6
80 – 100	0.7647	1.2	0.7761	1.0	0.7674	1.0	0.7697	0.6
100 – 120	0.6983	1.4	0.6987	1.1	0.6870	1.1	0.6942	0.7
120 – 150	–	–	0.6768	1.0	–	–	0.6768	1.0
150 – 175	–	–	0.6665	1.1	–	–	0.6665	1.1
175 – 200	–	–	0.6459	1.1	–	–	0.6459	1.1
200 – 225	–	–	0.6432	1.6	–	–	0.6432	1.6
30 – 80	0.9108	1.1	0.9460	0.8	0.9342	0.9	0.9317	0.5
Evaluation 2								
5 – 7.5	0.6279	7.7	0.8725	6.9	0.7223	5.3	0.7436	3.7
7.5 – 10	0.8350	4.7	0.8470	5.3	0.8469	3.9	0.8432	2.6
10 – 12.5	0.7715	3.6	0.8246	4.1	0.7809	3.1	0.7888	2.0
12.5 – 15	0.8310	3.0	0.9068	3.2	0.8393	2.6	0.8544	1.7
15 – 20	0.8291	1.9	0.8312	2.1	0.8532	1.6	0.8400	1.1
20 – 25	0.9563	1.5	0.9986	1.6	0.9907	1.3	0.9822	0.8
25 – 30	0.9103	1.3	0.9369	1.3	0.9158	1.1	0.9204	0.7
30 – 40	0.9171	1.1	0.9441	1.0	0.9422	1.0	0.9358	0.6
40 – 50	0.9745	1.1	0.9946	1.0	0.9913	1.0	0.9876	0.6
50 – 60	0.9019	1.1	0.9245	1.0	0.9161	1.0	0.9147	0.6
60 – 80	0.7935	1.0	0.8129	0.9	0.8029	0.9	0.8037	0.5
80 – 100	0.7508	1.1	0.7554	0.9	0.7487	0.9	0.7516	0.5
100 – 120	0.6924	1.2	0.6805	1.0	0.6746	1.0	0.6814	0.6
120 – 150	–	–	0.6558	0.9	–	–	0.6558	0.9
150 – 175	–	–	0.6417	1.0	–	–	0.6417	1.0
175 – 200	–	–	0.6263	1.0	–	–	0.6263	1.0
200 – 225	–	–	0.6183	1.5	–	–	0.6183	1.5
30 – 80	0.8968	0.9	0.9190	0.7	0.9131	0.8	0.9105	0.5

Table 10: THE NEUTRON CAPTURE CROSS SECTION OF ^{232}Th

Energy Bin (keV)	$\frac{\sigma(^{232}Th)}{\sigma(^{197}Au)}$	Uncertainty (%) stat	sys	tot	$\sigma(^{197}\mathrm{Au})^a$ (mb)	$\sigma(^{232}\mathrm{Th})$ (mb)
5 – 7.5	0.7436	3.7	1.6	4.0	1726.7	1283.9
7.5 – 10	0.8432	2.6	1.6	3.1	1215.7	1025.2
10 – 12.5	0.7888	2.0	1.6	2.6	1066.7	841.5
12.5 – 15	0.8544	1.7	1.6	2.3	878.0	750.2
15 – 20	0.8400	1.1	1.6	1.9	738.8	620.5
20 – 25	0.9822	0.8	1.6	1.8	600.0	589.4
25 – 30	0.9204	0.7	1.6	1.7	570.8	525.4
30 – 40	0.9358	0.6	1.6	1.7	500.4	468.3
40 – 50	0.9876	0.6	1.6	1.7	433.3	428.0
50 – 60	0.9147	0.6	1.6	1.7	389.6	356.4
60 – 80	0.8037	0.5	1.6	1.7	349.4	280.8
80 – 100	0.7516	0.5	1.6	1.7	298.3	224.2
100 – 120	0.6814	0.6	1.6	1.7	290.1	197.7
120 – 150	0.6558	0.9	1.6	1.8	274.1	179.8
150 – 175	0.6417	1.0	1.6	1.9	263.7	169.2
175 – 200	0.6263	1.0	1.6	1.9	252.6	158.2
200 – 225	0.6183	1.5	1.6	2.2	248.5	153.6

[a] Based on the ^{197}Au data from literature [18, 19].

5 DISCUSSION OF UNCERTAINTIES

Since the determination of statistical and systematic uncertainties in measurements with the 4π BaF_2 detector has been described extensively [9, 10, 12], this section deals mainly with the particular aspects of the present experiment. The various uncertainties are compiled in Table 11.

As shown in Fig. 3 the background from scattered neutrons is rather low due to the favorable cross section ratio for neutron scattering and capture in ^{232}Th. Furthermore, the low binding energy of thorium allows to use the full sum energy range from 5 to 10 MeV for normalizing the scattering background measured with the graphite sample. Accordingly, systematic uncertainties can be excluded in this context. Though the high background from the radioactivity of the sample presents a severe problem, it could be mastered by means of the good resolution in γ-ray energy and the high efficiency of the 4π BaF_2 detector. These features were essential for determining the cross section shape, since they allowed to select a well-defined window containing the sum energy peak at 4.8 MeV, well above the background that extends to 3.96 MeV. As demonstrated in Figs. 6 and 9, this window contains still more than 40% of the capture events but is not affected by background. Hence, the related uncertainties are practically negligible.

The contributions from the flight path uncertainty and from the normalization to equal neutron exposure have been discussed previously and are given in Table 11.

The thorium samples are specified with 99.5% purity. All remaining contaminants have

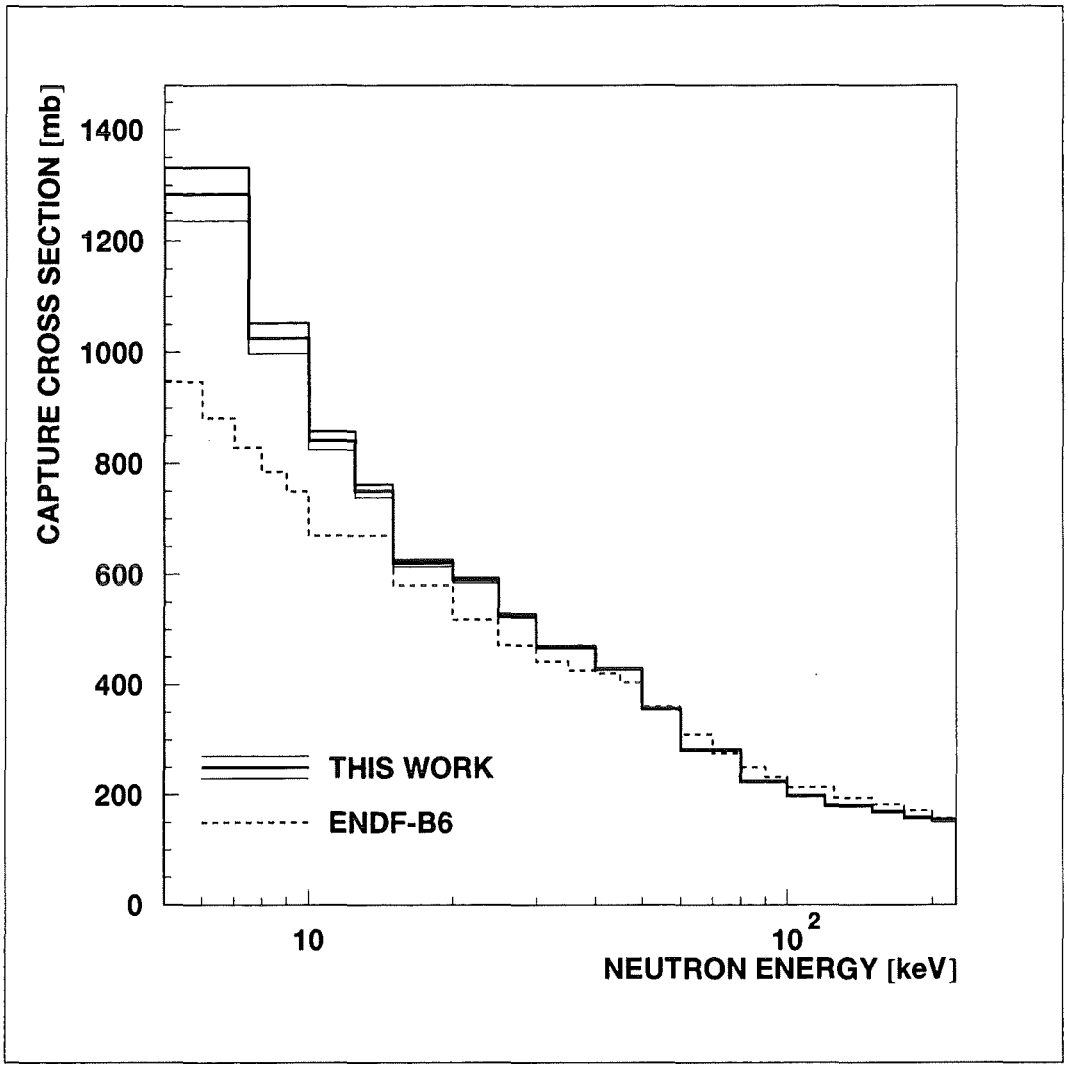

Figure 10: The neutron capture cross sections of ^{232}Th compared to the ENDF-B6 evaluation.

significantly smaller capture cross sections, resulting in almost negligible uncertainties. Since oxidation of the sample could also be excluded (in Sec. 2), a systematic uncertainty of 0.5% for the sample mass was considered a reasonable estimate.

In the present experiment, a small systematic difference between Evaluation 1 and Evaluation 2 was observed for the first time, which is probably due to the low binding energy of thorium. Since the statistical uncertainties of the mean values are 0.5%, this difference of 2.3% averaged over the three runs corresponds to more than two standard deviations. Correspondingly, a systematic uncertainty of 1% was assumed to account for this effect.

The systematic uncertainties of the correction for multiple scattering and self-shielding were calculated by the SESH code. These uncertainties could be directly adopted since the samples were isotopically pure and since the total and capture cross sections of thorium and gold could be perfectly reproduced with the adopted input parameters. Furthermore, the data obtained with samples of different thickness did not show any systematic

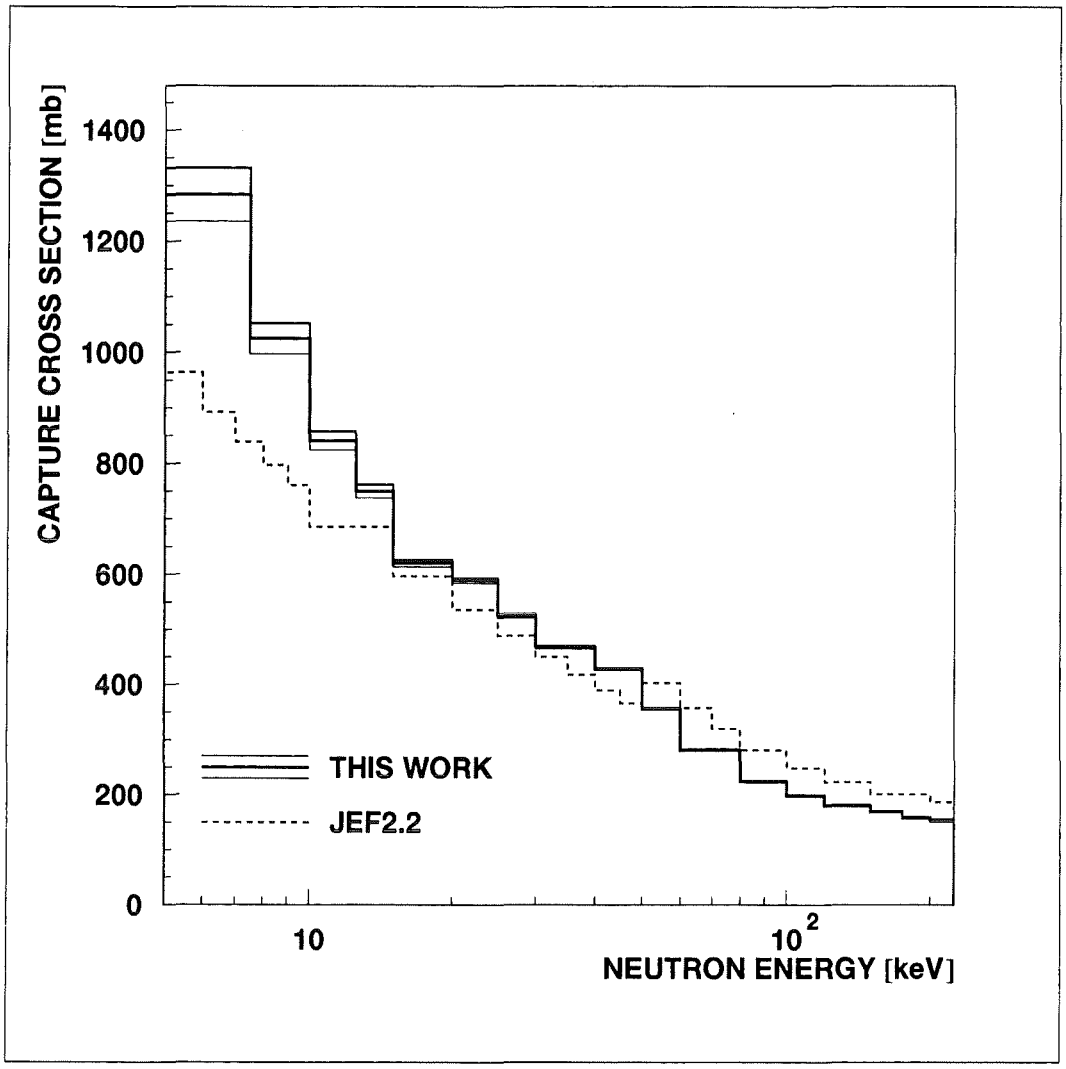

Figure 11: The neutron capture cross sections of ^{232}Th compared to the JEF2.2 evaluation.

differences.

A detailed discussion of systematic uncertainties due to undetected events was presented at the example of a measurement on a series of gadolinium isotopes [21]. There, the correction factor F_1 was found to show uncertainties of 0.3% for the even and of 0.8% for the odd isotopes. Based on two independent sets of calculated capture cascades, these estimates were in agreement with the respective uncertainties quoted in previous measurements with the 4π BaF_2 detector [9, 10, 17]. In a recent experiment [22] it was further verified that the same results were obtained when the calculated cascades were replaced by the capture cascades that were experimentally determined in the respective runs with the ADC system. It turned out that this uncertainty is related to the difference in binding energy between the investigated isotope and the gold standard. In Gd, this difference is large for the odd, but small for the even isotopes. The binding energy of thorium being 1.7 MeV lower than that of gold, implies the same but opposite difference as for the odd gadolinium isotopes. Therefore an uncertainty of 0.8% was assigned for this correction.

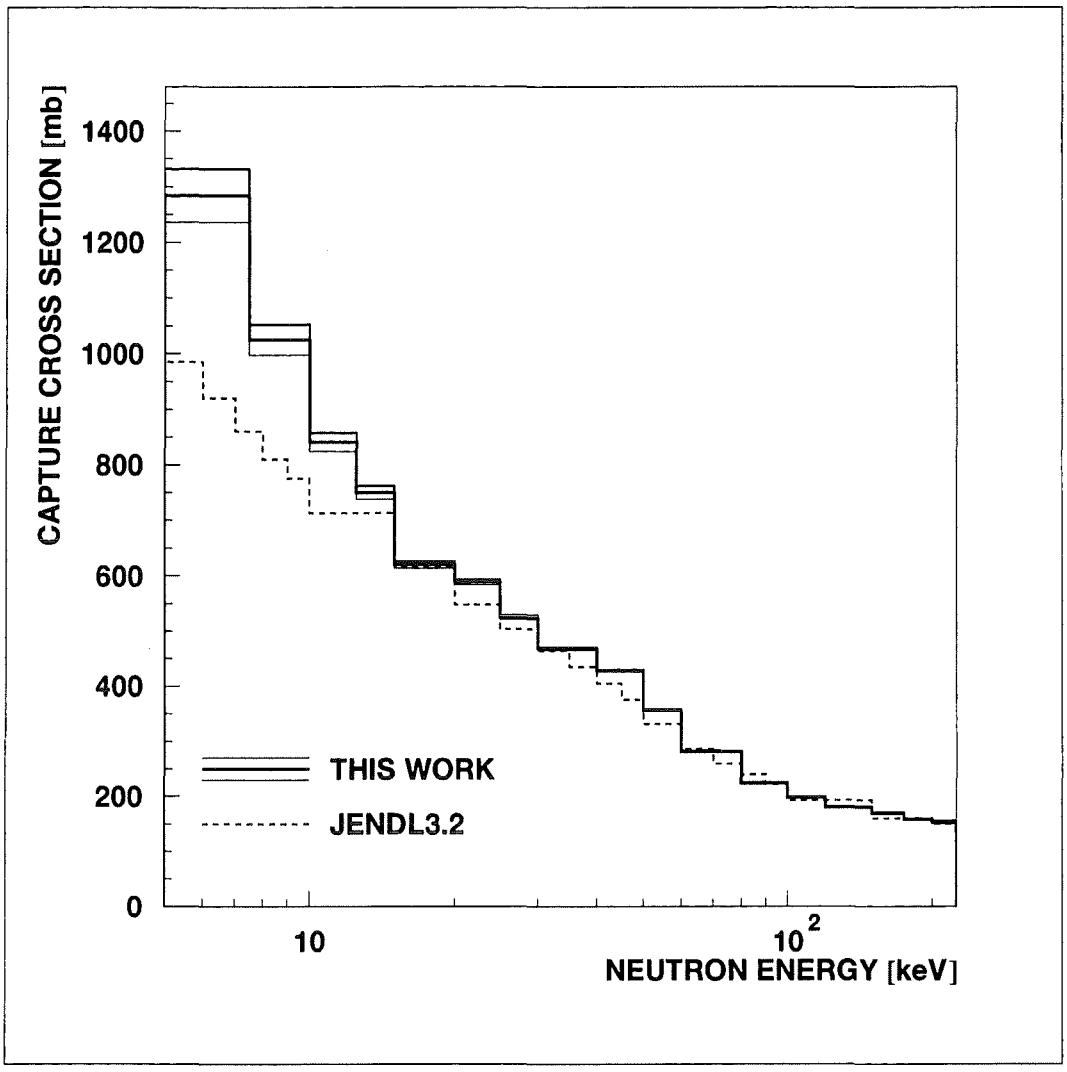

Figure 12: The neutron capture cross sections of ^{232}Th compared to the JENDL3.2 evaluation.

The uncertainty of the correction factor F_3 was estimated to 0.5%, consistent with the shift of the sum energy peak in the normalization window. This value is justified since the final cross sections at low energies are mainly determined by the runs with 100 keV maximum neutron energy, where the correction is small.

6 SUMMARY

The neutron capture cross section of ^{232}Th has been measured in the energy range from 5 to 225 keV at the Karlsruhe 3.75 MV Van de Graaff accelerator with uncertainties between 2.2 and 4.3% as requested for reactor applications. The present data set differs from previous works since it was obtained with a novel and independent technique based on the Karlsruhe 4π BaF_2 detector. With this setup, true capture events could be unambiguously

Table 11: SYSTEMATIC UNCERTAINTIES (%)

Flight path	0.1
Neutron flux normalization	0.2
Sample mass: elemental impurities and oxygen	0.5
Difference evaluation1/evaluation2:	1.0
Multiple scattering and self–shielding: F_2 cross section ratio	0.5
Undetected events: F_1 cross section ratio	0.8
Energy shift: F_3 cross section ratio	0.5
total systematic uncertaintiy $\sigma(^{232}\mathrm{Th})/\sigma(\mathrm{Au})$	1.6

separated from backgrounds caused by the neutron beam and from the radioactivity of the sample. The spectroscopic features of the detector allowed to minimize the necessary corrections and to evaluate systematic uncertainties in the most quantitative way. Hence, a new level of accuracy and reliability could be reached in the present experiment.

7 ACKNOWLEDGEMENT

We would like to thank our colleagues from IRMM Geel, F. Corvi and P. Mutti, for providing us with the thorium samples used in these measurements.

References

[1] S. Raman, C.W. Nestor, and J.W.T. Dabbs, in *Nuclear Cross Sections and Technology*, eds. R.A. Schrack and C.D. Bowman, NBS Spec. Pub. 425, (National Bureau of Standards, Washington D.C., 1975), Vol I, p. 222.

[2] C. Rubbia et al. 1995, Report CERN/AT/95-53(ET).

[3] F. Venneri et al. 1998, Report LA-UR-98-608, Los Alamos National Laboratory.

[4] C.D. Bowman, Annu. Rev. Nucl. Part. Sci. **48**, 505 (1998).

[5] C. Rubbia et al. 1998, Report CERN/LHC/98-02(EET).

[6] B.D. Kuzminov and V.N. Manokhin, in *Nuclear Data for Science and Technology*, eds. G. Reffo, A. Ventura, and C. Grandi, (Italian Physical Society, Bologna, 1997), Part II, p. 1167.

[6] K. Kobayashi, Y. Fujita, and N. Yamamuro, Journal of Nuclear Science and Technology **18**, 823 (1981).

[7] R.L. Macklin and J. Halperin, Nucl. Sci. and Eng. **64**, 849 (1977).

[8] R.L. Macklin and R.R. Winters Nucl. Sci. and Eng. **78**, 110 (1981).

[9] K. Wisshak, K. Guber, F. Voss, F. Käppeler, and G. Reffo, Phys. Rev. C **48**, 1401 (1993).

[10] K. Wisshak, F. Voss, F. Käppeler, and G. Reffo, Phys. Rev. C **45**, 2470 (1992).

[11] K. Wisshak, K. Guber, F. Käppeler, J. Krisch, H. Müller, G. Rupp, and F. Voss, Nucl. Instr. Meth. A **292**, 595 (1990).

[12] K. Wisshak, F. Voss, F. Käppeler, and G. Reffo, Phys. Rev. C **42**, 1731 (1990).

[13] F. H. Fröhner, 1968, Report GA-8380, Gulf General Atomic.

[14] K. Wisshak, F. Voss, F. Käppeler, L. Kazakov, and G. Reffo, Report FZKA 5967, Forschungszentrum Karlsruhe, Karlsruhe, Germany 1997.

[15] A. Gilbert and A.G.W. Cameron, Can. J. Phys. **43**, 1446 (1965).

[16] J. F. Mughabghab, M. Divadeenam, and N. E. Holden, *Neutron Cross Sections, Vol. 1, Part A* (Academic Press, New York, 1981).

[17] F. Voss, K. Wisshak, K. Guber, F.Käppeler, and G. Reffo, Phys. Rev. C **50**, 2582 (1994).

[18] R. L. Macklin, private communication (unpublished).

[19] W. Ratynski and F. Käppeler, Phys. Rev. C **37**, 595 (1988).

[20] V. McLane, C.L. Dunford, and P.F. Rose, *Neutron Cross Sections, Vol. 2,* (Academic Press, New York, 1988).

[21] K. Wisshak, F. Voss, F. Käppeler, K. Guber, L. Kazakov, N. Kornilov, M. Uhl, and G. Reffo, Phys. Rev. C. **52**, 2762 (1995).

[22] F. Voss, K. Wisshak, C. Arlandini, F. Käppeler, L. Kazakov, and T. Rauscher, Phys. Rev. C **59**, 1154 (1999).